Antenna Domain Mobility and Enzymatic Reaction of L-Rhamnulose-1-phosphate Aldolase[†,‡]

Dirk Grueninger and Georg E. Schulz*

Institut für Organische Chemie und Biochemie, Albert-Ludwigs-Universität, Albertstrasse 21, 79104 Freiburg im Breisgau, Germany

Received June 29, 2007; Revised Manuscript Received November 8, 2007

ABSTRACT: The enzyme L-rhamnulose-1-phosphate aldolase from *Escherichia coli* participates in the degradation pathway of L-rhamnose, a ubiquitous deoxy-hexose. It is a homotetramer of the rare C_4-symmetric type with N-terminal domains protruding like antennas from the main body. A mobility analysis of the enzyme gave rise to the hypothesis that an anisotropic thermal antenna motion may support the catalysis (Kroemer et al., Biochemistry *42*, 10560, 2003). We checked this hypothesis by generating four single mutants and one disulfide bridge that were designed to reduce the mobility of the antenna domain without disturbing the chain-fold or the active center. The catalytic rates of the mutants revealed activity reductions that correlated well with the expected antenna fixation. Among these mutants, K15W was crystallized, structurally elucidated, and used as a guide for modeling the others. The structure confirmed the design because the mutation introduced a tight nonpolar contact to a neighboring subunit that fixed the antenna but did not affect the main chain. The fixation was confirmed by a comparison of the anisotropic *B*-factors describing the mobility of the domains. It turned out that the distinctly anisotropic mobility of the wild-type antenna domain has become isotropic in K15W, in agreement with the design. We suggest that, like K15W, the other mutations also followed the design, validating the correlation between antenna mobility and activity. This correlation suggests that the domain mobility facilitates the reaction.

Aldolases are C−C bond-forming lyases catalyzing the aldol addition of aldehydes to activated carbons (*1*). Aldolases come in two classes: Class I uses a lysine residue to form a Schiff-base intermediate with a carbonyl carbon (*2*) whereas class II applies a divalent metal ion as an electron sink for the activation of a substrate enediolate intermediate (*3*, *4*). We are here concerned with the class II enzyme L-rhamnulose-1-phosphate aldolase from *Escherichia coli* (*5*, *6*) (RhuA,[1] EC 4.1.2.19), which is homologous to L-fuculose-1-phosphate aldolase (*7*, *8*) and to L-ribulose-5-phosphate 4-epimerase (*9*, *10*). RhuA participates in the degradation pathway of L-rhamnose (*11*) which is a ubiquitous sugar in prokaryotes and plants (*12*, *13*). The enzyme depends on Zn^{2+} and cleaves L-rhamnulose-1-phosphate (R1P) into L-lactaldehyde and dihydroxyacetone phosphate (DHAP) (Figure 1). In the reverse direction, RhuA can be used for C−C bond formation, creating two new chiral centers, which is an attractive feature for the enzymatic synthesis of novel compounds (*14*−*18*).

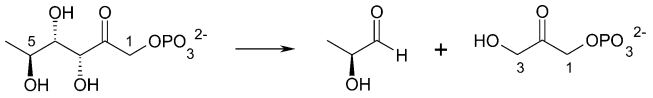

FIGURE 1: Reaction catalyzed by RhuA shown in the direction that was used in the enzymatic assay. The emergence of DHAP was monitored by NADH oxidation.

RhuA is a homotetramer showing the rare C_4 rather than the common D_2 point group symmetry (Figure 2A). One subunit has 274 amino acids with a polypeptide mass of 30145 Da. The chain forms a central nine-stranded β-sheet with a topological switch between β5 and β6 dividing the subunit into two domains (*5*). The N-terminal domain (residues 1−117) protrudes like an antenna into the solvent whereas the C-terminal domain (118−274) forms most of the tetramer interface and thus the core of the enzyme (Figure 2B). Moreover, the C-domain provides the three histidines fixing the Zn^{2+} ion at the active center (Figure 2C). On the basis of the structure of a complex with the inhibitor phospho-glycolohydroxamate at 2.7 Å resolution, on a 1.35 Å resolution structure of RhuA with a bound phosphate and on kinetic measurements of mutants, the catalytic mechanism of RhuA has been established (*5*, *6*). During catalysis, DHAP backed up by the crucial base Glu117 and bound to the N-domain (Figure 2C) contacts the Zn^{2+} ion in the C-domain and also the aldehyde, which is most likely bound to the C-domain (*6*, *8*) as indicated in Figure 2C.

Whereas domain movements caused by substrate binding are well-established features of enzymes (*19*, *20*), the support

[†] This work was supported by the Deutsche Forschungsgemeinschaft under grant SFB-388.

[‡] The atomic coordinates and structure factors have been deposited in the Protein Data Bank as entries 2V29, 2V2A, and 2V2B.

* To whom correspondence should be addressed. Tel: +49-761-203-6058, fax: +49-761-203-6161, e-mail: georg.schulz@ocbc.uni-freiburg.de.

[1] Abbreviations: CSC, triple mutant S59C-C126S-D191C of RhuA; DHAP, dihydroxyacetone phosphate; DTNB, *S*,*S*′-bis(5-thio-2-nitrobenzoate); GAAA, mutant K248G-R253A-E254A-E192A of RhuA; R1P, L-rhamnulose-1-phosphate; RhuA, L-rhamnulose-1-phosphate aldolase from *Escherichia coli*; TNB, 5-thio-2-nitrobenzoate.

10.1021/bi7012799 CCC: $40.75
Published on Web 12/18/2007

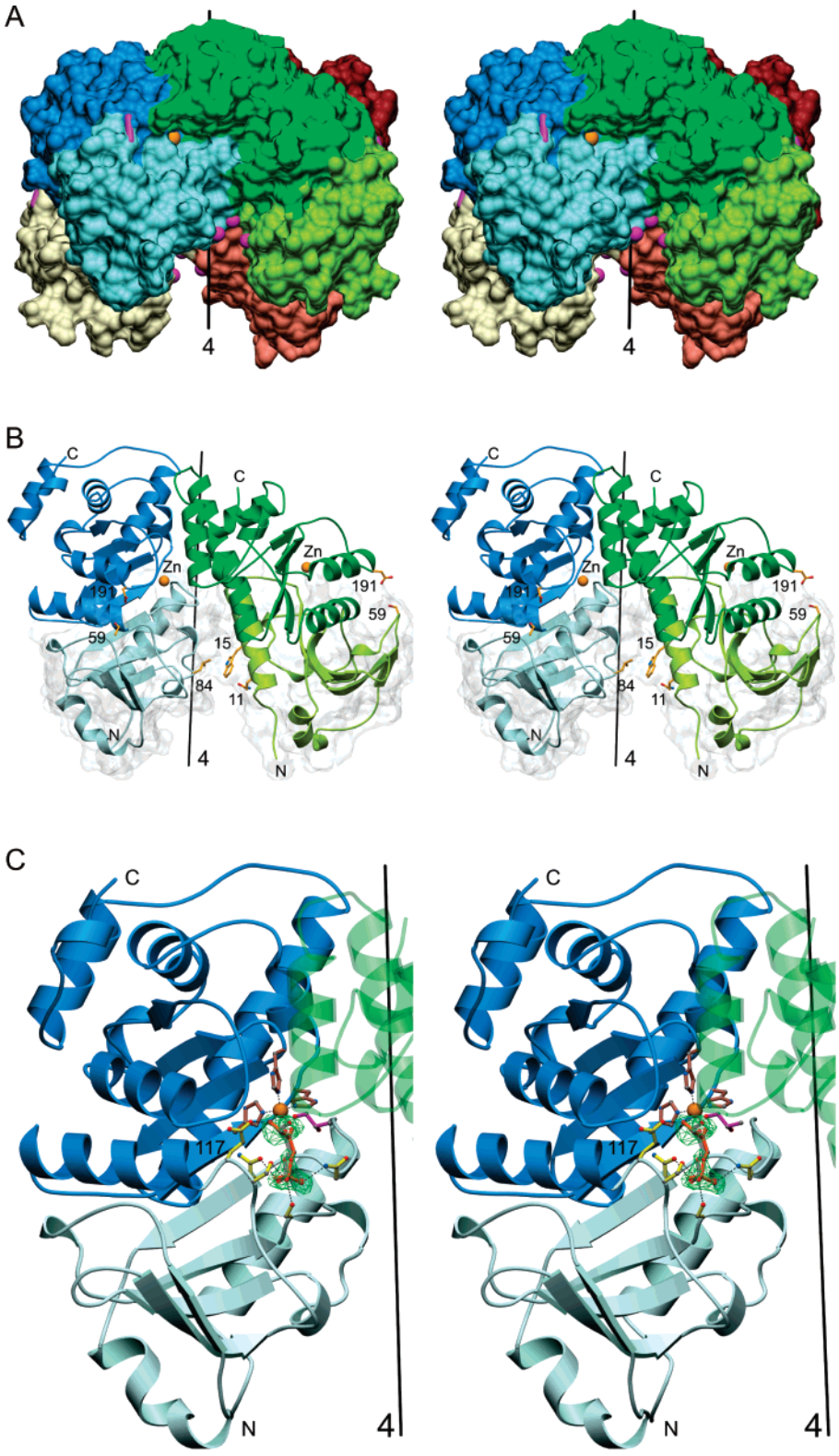

FIGURE 2: Stereoviews of the C_4-symmetric RhuA with its molecular fourfold axis. (A) Surface representation of RhuA colored by subunit. The N-domains have lighter colors than the C-domains. The Cβ atoms of the mutated residues at positions 11, 15, and 84 are given as pink balls. The disulfide bridge 59−191 of mobility mutant CSC is represented by a pink bar (Cβ−Cβ). The Zn^{2+} ion is orange. (B) Ribbon plot of two adjacent subunits showing the Zn^{2+} ions and the mutated residues. The mutation K15W is introduced. The N-terminal domain surfaces are given in a transparent mode. (C) The active center between the domains showing the Zn^{2+} ion held by three histidines from the C-terminal domain and DHAP held by several residues of the N-terminal antenna domain. DHAP was taken from the structure of the crystallization mutant GAAA soaked with R1P. Its (F_o − F_c)-difference electron density is given at the 3.0 σ contour level (green). An observed second conformation of DHAP is most likely unnatural (*6*, *8*) and shown in transparent gray. The aldehyde (pink) is depicted at its putative site (*6*, *8*) at the C-terminal domains of two neighboring subunits (blue and transparent green).

of the catalysis by thermal domain movements is the subject of a controversial discussion (*21*−*33*). With respect to RhuA, a high-resolution structure revealed an anisotropic mobility of the N-terminal domain, which was proposed to facilitate

catalysis (*6*). Similar domain movements were also suggested for the homologous enzyme L-fuculose-1-phosphate aldolase (*4*). Here we report enzyme kinetic data together with three crystal structures that show a correlation between the mobility of the N-domain and the catalytic activity.

MATERIALS AND METHODS

Mutagenesis and Activity Assay. The mutations were introduced using QuikChange (Stratagene, Heidelberg) and verified by DNA-sequencing (SeqLab, Göttingen). The oligonucleotides were synthesized by Qiagen (Hilden, Germany). RhuA and its mutants were overexpressed in *E. coli* JM105 and purified as described (*5*), except that the hydroxylapatite column was replaced by a size-exclusion column (Superdex 200, Pharmacia). This column was run with buffer A (20 mM Tris-HCl pH 7.2, 150 mM NaCl, 1 mM $ZnCl_2$, 10 mM β-mercaptoethanol). The resulting protein was dialyzed against 10 mM β-mercaptoethanol and concentrated to 20 mg/mL.

In order to introduce the disulfide bridge 59−191, we dialyzed a 10 μM solution of the triple mutant S59C-C126S-D191C (mutant CSC) for 48 h against buffer B (20 mM Tris-HCl pH 7.2, 150 mM NaCl and 1 mM $ZnCl_2$). The thiols were oxidized by adding *S,S*′-bis(5-thio-2-nitrobenzoate) (DTNB, Fluka, Deisenhofen, Germany) over 90 min up to a four-fold molar excess. During the titration the solution turned yellow, which agreed qualitatively with the expected reduction of colorless DTNB to yellow 5-thio-2-nitrobenzoate (TNB) on disulfide formation. After 6 h incubation at room temperature, a further dialysis over 20 h against buffer B was performed to remove the reagent DTNB and the product TNB. For rereduction the protein solution was incubated for 30 h at room temperature with 20 mM β-mercaptoethanol. The DTNB-oxidized enzyme was analyzed by nonreducing SDS-PAGE and by ESI-MS (error range 5 Da), which ruled out an intermolecular disulfide bond as well as enzyme-bound TNB or β-mercaptoethanol.

The substrate R1P was produced as described (*34*). The enzymatic activity was determined photometrically in a coupled assay at 37 °C. The cuvette contained 0.2 mM NADH and 0.25−5 mM R1P as well as 5 units of glycerol-3-phosphate dehydrogenase (Sigma, Steinheim, Germany) in buffer D (60 mM Tris-HCl pH 7.5, 60 mM KCl). The reaction was started by adding 30 μg of the respective RhuA species dissolved in buffer B, and the NADH absorption at 366 nm was monitored over about 1 min.

Structure Analyses. Crystallization of RhuA mobility mutant K15W was carried out at 20 °C using the hanging drop method. The drops consisted of 2 μL of a 12 mg/mL protein solution and 2 μL of the reservoir (100 mM sodium acetate pH 4.5, 50% (v/v) ethylene glycol and 5% (w/v) PEG 1000). Within 7 days the crystals grew to dimensions of 180 × 110 × 70 μm^3. The crystals of surface mutant GAAA (K248G-R253A-E254A-E192A) and those of the combined mutant GAAA-E117S were produced by the same method but with a reservoir solution of 40% (v/v) 1,2-propanediol, 50 mM calcium acetate, and 100 mM sodium acetate at pH 4.5. They grew to maximum dimensions of 240 × 80 × 80 μm^3 and were soaked for 24 h with 10 mM R1P.

For X-ray analysis, all crystals were shock-frozen at 100 K in a nitrogen gas stream. X-ray diffraction data were collected at DESY (Hamburg) and at the SLS (Villigen, Switzerland) and processed with XDS (*35*). The initial protein models were obtained by molecular replacement using the program CNS (*36*) with the RhuA wild-type structure as search model (code 1GT7). The protein models were improved with COOT (*37*). Water molecules were added and the structures were refined using CNS (*36*). All three structures were subjected to a final refinement using REFMAC5 (*38*) with the N- and C-terminal domains defined as two TLS groups (*39*). The TLS parameters were analyzed with TSLANL (*40*). The figures were prepared using POVscript (*41*) and POVRAY (http://www.povray.org). The side chain conformation of the mobility mutant K15W turned out as one of the preferred rotamers listed in COOT (*37*). For mutants Q11W, L84W, and K15Y we checked all listed rotamers (*37*), most of which were impossible for steric reasons. Among the remaining rotamers we chose those with the lowest solvent-exposed nonpolar surface.

RESULTS

Mobility Mutants. The 1.35 Å resolution structure of RhuA revealed a *B*-factor anisotropy in the N-terminal antenna domain that showed a preferred rotational mobility around the molecular 4-fold axis (*6*). Because the active center is located between the N- and C-domain of each subunit (Figure 2C), the corresponding azimuthal rotation seems likely to affect the catalysis. In order to investigate the connection between the mobility of the N-antenna domain and catalysis, we generated a set of mutants designed to diminish the antenna mobility without affecting the structure itself. We chose the surface residues Gln11, Lys15, and Leu84, which are located between neighboring antenna domains (Figure 2), and replaced them with the more voluminous residues tryptophan and tyrosine in order to diminish the azimuthal mobility (Figure 3). Being at the surface, the amino acid exchanges are not expected to change the structure. Moreover, they are unlikely to disturb the active center, because they are more than 20 Å away from the Zn^{2+} ion.

Furthermore, we generated a disulfide bond between position 59 of the N-domain and position 191 of the C-domain. For this purpose, we produced the triple mutant S59C-C126S-D191C (CSC) and oxidized the introduced thiols to form a disulfide bridge. The additional mutation C126S was necessary because Cys126 is at the surface and may form false intermolecular disulfides. The other two thiols of Cys142 and Cys172 are deeply buried and certainly unavailable for DTNB. The designed disulfide constitutes a fix point where the two domains are tied together, reducing the antenna mobility (Figure 2). The bridge introduced some strain because the 59-Cβ to 191-Cβ distance is 6 ± 1 Å in the known RhuA structures, which is about 1.5 Å longer than the respective distance in a disulfide bridge. However, the distance between the bridge and the Zn^{2+} ion is 16 Å, so that the disturbance of the active center should be negligible.

Structures of Mutants K15W, GAAA, and GAAA-E117S. In order to establish structural detail, we crystallized the mobility mutant K15W (Table 1) and obtained a well-ordered new crystal form. The structure was established using the molecular replacement method revealing two closely similar RhuA subunits per asymmetric unit. The resulting model was

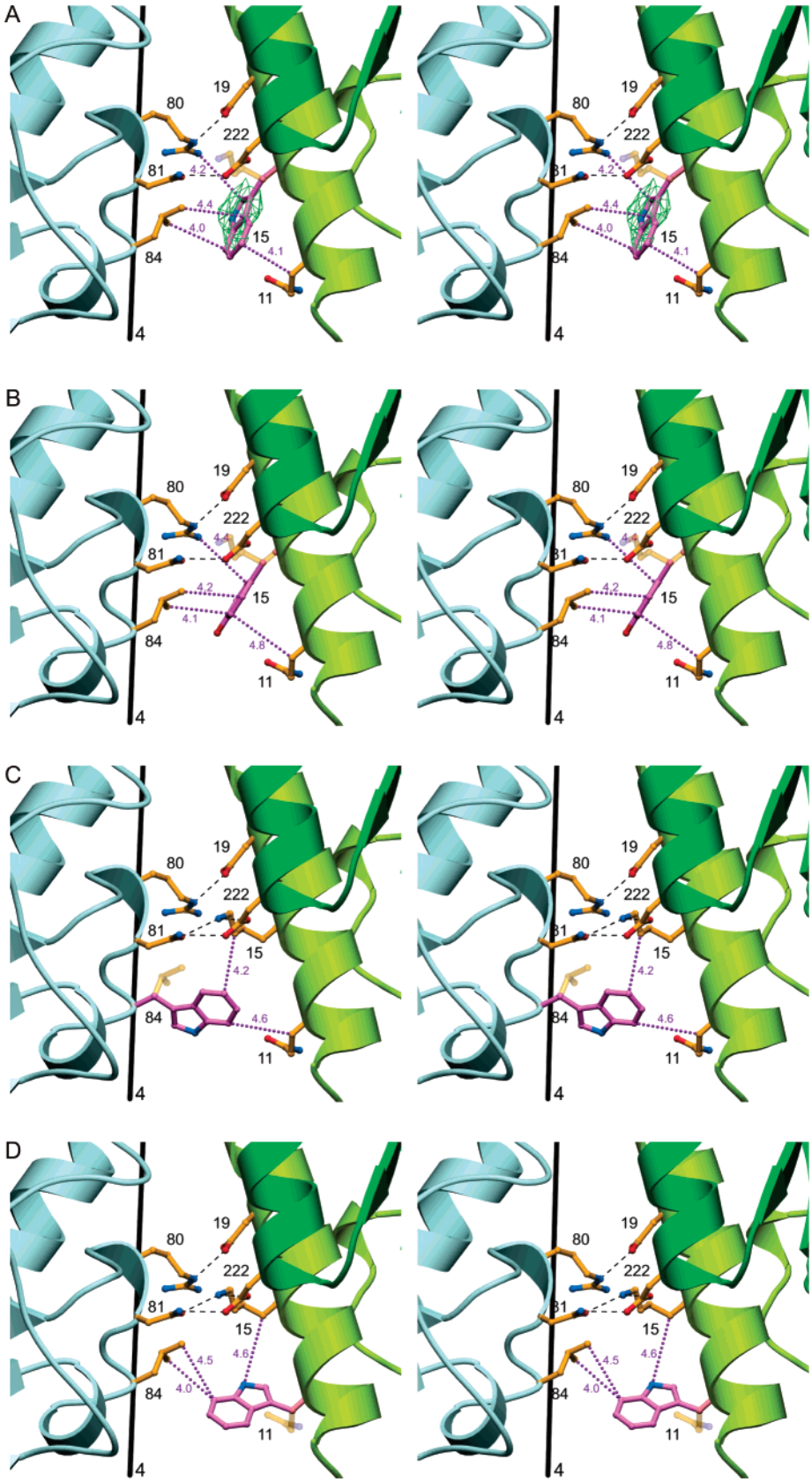

FIGURE 3: Stereoview of the structures around the mutated residues. The newly introduced side chains are pink. The original side chains are shown in a transparent mode. (A) Structure of mutant K15W. Trp15 adopts one of the rotamer conformations listed in COOT (*37*) and contacts Leu84. The ($F_o - F_c$)-difference electron density for the side chain of Trp15 is given at the 2.5 σ contour level (green). (B) Model of mutant K15Y selecting the rotamer (*37*) that made no clashes and exposed the smallest nonpolar surface to the solvent. (C) Model of mutant L84W using the same selection criteria as for K15Y. (D) Model of mutant Q11W using the same selection criteria as for K15Y.

refined (Table 1). The ($F_o - F_c$)-difference electron density map (Figure 3A) showed clear density for the newly introduced Trp15 in one of the preferred rotamer conformations listed in COOT (*37*). Trp15 made a close 4.0 Å contact

Table 1: Data Collection and Refinement[a]

	K15W	GAAA[b]	GAAA-E117S[b]
	Data Collection		
wavelength (Å), source	0.8123, DESY	0.9000, SLS	0.9050, SLS
resolution range (Å)	50−2.0	10−1.75	50−1.5
unique reflections	44803 (5871)	30749 (1810)	44912 (4655)
completeness (%)	100 (100)	92.6 (44.6)	87.9 (78.5)
multiplicity	4.3 (4.2)	7.0 (5.2)	3.9 (2.5)
I/σ_I	12.3 (4.2)	23.0 (11.4)	17.1 (2.7)
R_{sym-I} (%)	8.1 (35)	5.8 (11)	4.0 (32)
space group	*P*4[c]	$P42_12$	*I*4
unit cell axes (Å)	82.9, 82.9, 98.1	106.3, 106.3, 56.4	84.2, 84.2, 91.7
Wilson-*B*-factor (Å^2)/solvent (%)	24/56	17/53	22/54
	Refinement		
R_{cryst}/R_{free} (7% test set)	0.161/0.197	0.147/0.172	0.166/0.184
no. of atoms: protein	4258	2268	2112
ligand	45[d]	22[e]	16[f]
solvent	365	277	217
average *B*-factor (Å^2)	25.8[c]	13.5	22.1
rmsd bond lengths (Å)/angles (deg)	0.015/1.35	0.010/1.25	0.010/1.40
Ramachandran: favored/allowed/disallowed (%)	90.6/9.2/0.2	90.5/9.5/0.0	91.8/8.2/0.0

[a] All structures were refined using the N-and C-domains as two TLS-groups. Values in parentheses are for the highest resolution shell. The additional Zn^{2+} ions remained bound to RhuA in the final dialysis step and ended in crystal contacts. [b] See text for mutant abbreviations. [c] The crystals contained two tetramers per unit cell, which showed a relative rotation of 18° around the two molecular fourfold axes. Both axes were crystallographic. The average *B*-factors for the two tetramers were approximately identical. [d] The number includes five Zn^{2+} ions, six ethyleneglycol and four acetate molecules. [e] The number includes two Zn^{2+} ions and two DHAP molecules. [f] The number includes two Zn^{2+} ions, one propandiol, one phosphate, and one acetate molecule.

to Leu84 of a neighboring subunit without changing either of the two backbones. Consequently, Trp15 reduced the mobility of the antenna domain but did not cause steric stress.

The crystals of GAAA and GAAA-E117S were originally produced in the hope that they would provide a new crystal form showing the binding site of the substrate R1P or of the products L-lactaldehyde or DHAP. In particular the aldehyde site had not yet been occupied in any crystal of RhuA (*5*, *6*) or of the closely homologous L-fuculose-1-phosphate aldolase (*8*). The experiment succeeded insofar as we found a bound DHAP molecule in the GAAA crystal and a bound phosphate in the GAAA-E117S crystal but nothing at the putative aldehyde site. The phosphate was bound at the same position as in previous structures (*4*, *6*). The DHAP molecule was refined in two conformations that deviated from each other only by the position of the 3-hydroxyl group (Figure 2C). The presumed natural conformation is identical to that of the inhibitor phospho-glycolohydroxamate (*4*, *6*), so that the analyses of GAAA and GAAA-E117S yielded no novel data on substrate binding. However, the two structures were most useful for the analysis of the domain motions (see below).

Enzyme Kinetics. The enzymatic activity values of the mobility mutants are given in Table 2. All produced mutants and the wild-type were checked by ESI-MS measurements. The observed deviations from the calculated values are given in Table 2. Since all deviations are negative, the calibration was probably offset by −5 Da. Assuming such an offset, the spread is only 3 Da demonstrating that there can be at most added or missing hydrogen atoms and no further modifications, in particular no modifications of the CSC mutants. The actual formation of the disulfide bridge was confirmed by the observed emergence of the TNB color.

The activity values are well explained by the position of the amino acid exchanges. Among the three mutated residues, Lys15 lies deepest in the cleft between the N-antenna domains of the tetramer (Figure 2B). This region is very crowded so that the effect on the mobility and consequently on the activity should be most severe. Accordingly, mutants K15W and K15Y exhibited the lowest activity. Residues 84 and 11 are further away from the core in a less crowded region between the antennas. This correlates well with the observation that the activity values are closer to those of the wild-type.

Table 2: Enzyme Kinetics of Mobility Mutants

enzyme species	deviation from calculated mass[a] [Da]	k_{cat}[b] [%]	K_M[b] [mM]
wild-type	−4	100[c]	2.0 ± 0.1
Q11W	−6	71 ± 5	1.9 ± 0.2
L84W	−4	40 ± 7	5.4 ± 1.1
K15Y	−5	9 ± 0.4	2.5 ± 0.3
K15W	−3	4 ± 0.2	2.0 ± 0.2
CSC reduced	−8	42 ± 2	1.4 ± 0.1
CSC oxidized	−7	4 ± 0.5	2.1 ± 0.4
CSC rereduced	−8	32 ± 2	2.0 ± 0.2

[a] Each mutant mass was determined by ESI-mass spectroscopy and compared with the respective calculated mass. The deviations are negligible and exclude any significant modifications involving non-hydrogen atoms. [b] The values for wild-type and single mutants are based on 30 measurements per enyzme species. The CSC values rely on 10 measurements per species. [c] The k_{cat} value for wild-type RhuA was determined to (9.1 ± 0.3) s^{-1} which corresponds to a specific activity of 18 units/mg.

Mutant CSC displayed a decrease in activity already in the reduced state of the disulfide (Table 2), which may be due to an undetected partial oxidation in the air. On disulfide bridge formation with DTNB, the antenna is fastened to the C-domain of the same subunit, constraining its mobility. This corresponds well with the observation that the oxidized mutant CSC exhibited a significant decrease in activity. Subsequent reduction with β-mercaptoethanol resulted in a reconstitution of the activity to 76% of the initial level (Table 2). The values for the reduced, oxidized, and rereduced

Table 3: Anisotropy of Domain Mobility[a]

	N-domain			C-domain		
	Δr	$r\Delta\varphi$	Δz	Δr	$r\Delta\varphi$	Δz
E192A	943	1090	967	961	1044	995
GAAA	853	1340	807	797	1254	949
GAAA-E117S	722	1127	1151	870	1099	1031
normalized avg ratio	100	142	119	100	130	109
K15W-A	945	1007	1048	925	1055	1020
K15W-B	959	1054	987	931	1065	1004
normalized avg ratio	100	108	107	100	114	109

[a] All numbers are normalized values which, except for E192A, were derived from refinements using the N- and C-domains as TLS-groups (Table 1). E192A was refined with individual anisotropic *B*-factors (*6*), which have now been averaged over each domain. The average ratios are normalized by setting the radial component to 100. The excess ratios ($r\Delta\varphi - \Delta r$) and ($\Delta z - \Delta r$) are plotted in Figure 4. Mutants E192A, GAAA, and GAAA-E117S were wild-type-like structures. K15W-A and K15W-B refer to the two independent molecules of the designed mobility mutant.

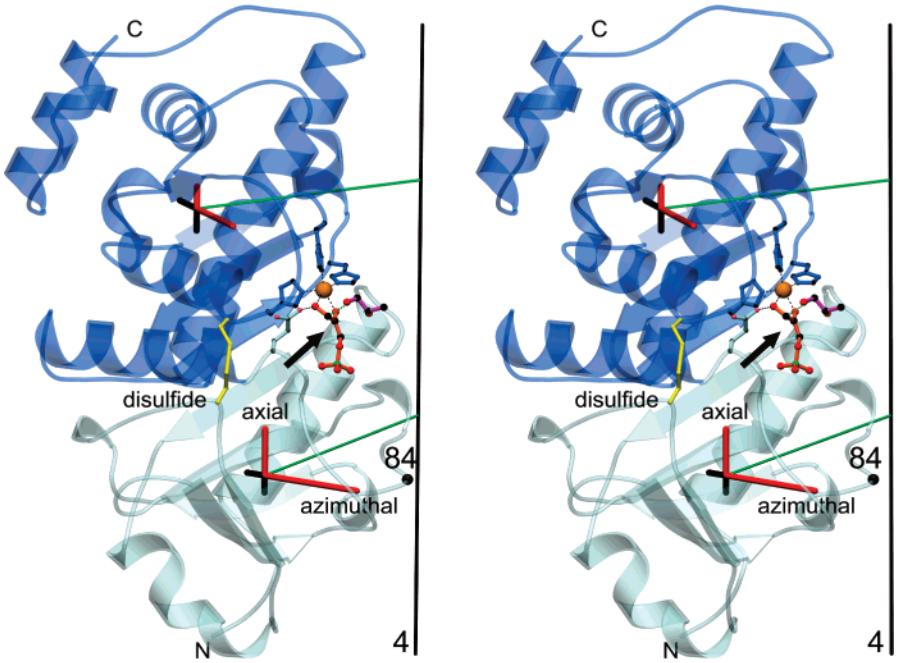

FIGURE 4: Stereoview illustrating the anisotropic mobility of the N-terminal antenna domain and of the C-terminal core domain. The chain-fold of one RhuA subunit is depicted in a transparent mode colored by domain. The anisotropic mobility is referred to cylindrical coordinates and plotted as bars at the center of mass of each domain. The lengths of the bars (red for the three wild-type-like structures, black for the two structures of mobility mutant K15W) correspond to the excess ($r\Delta\varphi - \Delta r$) and ($\Delta z - \Delta r$) over the isotropic part characterized by Δr (Table 3). The radial component Δr is always the smallest one. The figure shows the active center Zn^{2+} together with the three histidines, the substrate DHAP (only the relevant conformation (*4*, *6*) in orange), L-lactaldehyde (pink) at its putative position, Glu117 that forms a hydrogen bond to the oxygen of DHAP in the crystal but deprotonates the adjacent carbon atom during catalysis (*4*, *6*), the disulfide bond (59−191), and position 84 the side chain of which contacts the newly introduced tryptophan of mutant K15W. The arrow indicates the resulting direction of the mobility, which is almost in line with the bond formation/breakage.

enzyme demonstrate that the formation of the disulfide bridge drastically diminishes the activity.

It should be noted that all K_M values are in the same range (Table 2), except for L84W showing a limited increase. Since the K_M values did increase appreciably on tinkering with the substrate binding site (*6*), the enzyme shows the usual relationship between K_M and substrate affinity. Therefore, the comparatively constant K_M values suggest that the applied mutations and in particular the disulfide bridge did not disturb substrate binding. An electrostatic effect on removing a positive charge in mutant K15W is conceivable. However, the influence of the deleted charge is diminished by the long distance to the active center (Figure 2B) and also shielded off by salt bridge Arg80-Asp19, which is positioned between the mutation and the Zn^{2+} ion (Figure 3A). In conclusion, it is very unlikely that the observed activity reductions are caused by perturbations of the active center.

Mobility Derived from Crystal Structures. Presently, six independent structures of RhuA from *E. coli* are known: the four molecules of mutants K15W (chains A and B), GAAA, and GAAA-E117S reported here and, in addition, those of the wild-type (code 1GT7) (*5*) and of the surface mutant E192A (code 1OJR) (*6*). Mutations E192A and GAAA are all at the surface of the C-domain and far away from the active center. They were introduced for crystallization. RhuA mutant E192A was shown to be fully active (*6*). In general, all these structures show a higher mobility in the N-terminal antenna domain than in the C-domain. For a more detailed analysis, we excluded the wild-type structure because of its insufficient 2.7 Å resolution (*5*). This left us with the five structures of E192A (1.35 Å), K15W-A (2.0 Å), K15W-B (2.0 Å), GAAA (1.75 Å), and GAAA-E117S (1.5 Å) analyzed at the resolution stated in parentheses.

The resolution in the analysis of E192A was high enough to allow an anisotropic *B*-factor refinement (*6*). For this structure, we averaged the anisotropic *B*-factors of each Cα atom over the N-domain as well as over the C-domain, yielding the anisotropic *B*-factors for each domain. The three reported crystal structures were refined at a lower resolution than E192A (Table 1). However, the N- and C-terminal domains were defined as separate TLS-groups in order to focus on domain mobility. These refinements resulted in good quality indices (Table 1) and in anisotropic *B*-factors averaged over the N- and C-terminal domains. The resulting anisotropic domain mobility is usually represented in form of a mobility ellipsoid.

The mobility ellipsoids of all domains were interpreted in terms of their components (Δr, $r\Delta\varphi$, Δz) in a cylindrical coordinate system (r, φ, z) defined around the molecular four-fold z-axis. For each domain the components were then normalized in order to reduce unavoidable errors introduced by differing precision of the crystal packings. The results are listed in Table 3. For almost all domains, the radial mobility Δr was the smallest component and the azimuthal mobility $r\Delta\varphi$ was the largest. The spread of the normalized mobility values is rather broad (Table 3), which is readily explained by the influence of varying packing contacts. However, we have three structures of wild-type-like RhuA molecules (E192A, GAAA, and GAAA-E117S) and two RhuA molecules of the designed mobility mutant K15W. In order to demonstrate the effect of the designed mutation, we averaged over these two groups and normalized the result by setting all Δr values to 100. The anisotropy is then best described by the excess over the isotropic part. The excess is depicted for each domain in Figure 4. Clearly, the designed mobility mutation K15W nearly abolished the anisotropy of the N-antenna domain and diminished that of the C-core domain.

DISCUSSION

The dependence of a catalytic reaction on the mechanical properties of an enzyme structure was first established with the recognition of the induced-fit movements of hexokinase (*19*). As an increasing number of high-resolution crystal and detailed NMR (*22*) structures of enzymes become available, the correlation between the mechanical displacements along the reaction coordinate, for instance in a hydride transfer, and the Brownian motion of the solvent emerged as a central question (*23*, *24*, *27*, *30*, *33*). The funneling of the isotropic solvent motion into a directed displacement within the enzyme was analyzed by establishing the anisotropic mobility of various parts of proteins in crystal structures (*25*, *26*, *28*, *31*), by molecular dynamics calculations (*29*, *31*) and by enzyme modifications that changed the mechanical properties such as amino acid exchanges (*30*) or glycosylations (*29*).

Here we report designed mutants of a C_4-symmetric enzyme with four N-terminal antenna domains sticking out of a core formed by the C-terminal domains (Figure 2) in conjunction with activity measurements. For one of the mutants, K15W, the design was confirmed by a structure analysis that showed the introduction of a tight contact, rigidifying the antenna without disturbing the chain-fold. Assuming that the other mutants also followed the design (Figure 3), we found that introducing demanding side chains in more (K15W) or less (Q11W) crowded regions between the antenna domains reduced the activity accordingly. This shows a correlation between antenna mobility and enzymatic activity (Table 2). For mutant K15W, the correlation was confirmed by a structure analysis (Figure 4, Table 3). It should be noted that the activity of the structurally confirmed mutant K15W dropped by a factor of 25 (Table 2). This is a much larger effect than the reduction by a factor of 2 that was observed in a series of glycosylation experiments (*29*). Together, these data suggest that the mobility of the N-terminal domain facilitates the reaction. In view of the controversial discussion on the influence of thermal domain motions on catalysis (*21*−*33*), it seems likely that the directed antenna motion channels the bound substrates into a 'near attack conformation' reducing the entropic part of the activation energy (*27*).

ACKNOWLEDGMENT

We thank the teams of DESY (Hamburg) and of the SLS (Villigen, Switzerland) for their help in data collection and C. Warth for the ESI-MS measurements.

REFERENCES

1. Mehler, A. H., and Marshall, E. C., Jr. (1967) Aldolase reaction with sugar diphosphates, *Science 155*, 1101−1103.
2. Lorentzen, E., Siebers, B., Hensel, R., and Pohl, E. (2005) Mechanism of the Schiff base forming fructose-1,6-bisphosphate aldolase: Structural analysis of reaction intermediates, *Biochemistry 44*, 4222−4229.
3. Horecker, B. L., Tsolas, O., and Lai, C. Y. (1972) Aldolases, in *The Enzymes* (Boyer, P. D., Ed.) 3rd ed., Vol. 7, pp 213−258, Academic Press, New York.
4. Dreyer, M. K., and Schulz, G. E. (1996) Catalytic mechanism of the metal-dependent fuculose aldolase from *Escherichia coli* as derived from the structure, *J. Mol. Biol. 259*, 458−466.
5. Kroemer, M., and Schulz, G. E. (2002) The structure of L-rhamnulose-1-phosphate aldolase (class II) solved by low-resolution SIR phasing and 20-fold NCS averaging, *Acta Crystallogr., Sect. D: Biol. Crystallogr. 58*, 824−832.
6. Kroemer, M., Merkel, I., and Schulz, G. E. (2003) Structure and catalytic mechanism of L-rhamnulose-1-phosphate aldolase, *Biochemistry 42*, 10560−10568.
7. Dreyer, M. K., and Schulz, G. E. (1993) The spatial structure of the class II L-fuculose-1 phosphate aldolase from *Escherichia coli*, *J. Mol. Biol. 231*, 549−553.
8. Joerger, A. C., Mueller-Dieckmann, C., and Schulz, G. E. (2000) Structures of L-fuculose-1-phosphate aldolase mutants outlining motions during catalysis, *J. Mol. Biol. 303*, 531−543.
9. Luo, Y., Samuel, J., Mosimann, S. C., Lee, J. E., Tanner, M. E., and Strynadka, N. C. J. (2001) The structure of L-ribulose-5-phosphate 4-epimerase: An aldolase-like platform for epimerization, *Biochemistry 40*, 14763−14771.
10. Samuel, J., Luo, Y., Morgan, P. M., Strynadka, N. C. J., and Tanner, M. E. (2001) Catalysis and binding in L-ribulose-5-phosphate 4-epimerase: A comparison with L-fuculose-1-phosphate aldolase, *Biochemistry 40*, 14772−14780.
11. Badia, J., Baldolmà, L., Aguilar, J., and Boronat, A. (1989) Identification of the *rhaA*, *rhaB* and *rhaD* gene products from *Escherichia coli* K-12, *FEMS Microbiol. Lett. 65*, 253−258.
12. McNeil, M., Darvill, A. G., Fry, S. C., and Albersheim, P. (1984) Structure and function of the primary cell walls of plants, *Annu. Rev. Biochem. 53*, 625−663.
13. Graninger, M., Kneidinger, B., Bruno, K., Scheberl, A., and Messner, P. (2002) Homologs of the Rml enzymes from *Salmonella enterica* are responsible for dTDP-β-L-rhamnose biosynthesis in the Gram-positive thermophile *Aneurinibacillus thermoaerophilus* DSM 10155, *Appl. Environ. Microbiol. 68*, 3708−3715.
14. Bednarski, M. D., Simon, E. S., Bischofberger, N., Fessner, W.-D., Kim, M.-J., Lees, W., Saito, T., Waldmann, H., and Whitesides, G. M. (1989) Rabbit muscle aldolase as a catalyst in organic synthesis, *J. Am. Chem. Soc. 111*, 627−635.

15. Fessner, W.-D., Sinerius, G., Schneider, A., Dreyer, M., Schulz, G. E., Badia, J., and Aguilar, J. (1991) Diastereoselective enzymatic aldol additions: L-rhamnulose and L-fuculose-1-phosphate aldolases from *E. coli*, *Angew. Chem., Int. Ed. 30*, 555−558.
16. Wong, C.-H., Halcomb, R. L., Ichikawa, Y., and Kajimoto, T. (1995) Enzymes in organic synthesis: application to the problems of carbohydrate recognition, *Angew. Chem., Int. Ed. 34*, 412−432.
17. Espelt, L., Parella, T., Bujons, J., Solans, C., Joglar, J., Delgado, A., and Clapes, P. (2003) Stereoselective aldol additions catalyzed by dihydroxyacetone phosphate-dependent aldolases in emulsion systems: Preparation and structural characterization of linear and cyclic iminopolymers from aminoaldehydes, *Chem. Eur. J. 9*, 4887−4899.
18. Tanaka, F., Fuller, R., and Barbas, C. F., III. (2005) Development of small designer aldolase enzymes: Catalytic activity, folding, and substrate specificity, *Biochemistry 44*, 7583−7592.
19. Bennett, W. S., Jr., and Steitz, T. A. (1978) Glucose-induced conformational change in yeast hexokinase, *Proc. Natl. Acad. Sci. U.S.A. 75*, 4848−4852.
20. Vonrhein, C., Schlauderer, G. J., and Schulz, G. E. (1995) Movie of the structural changes during a catalytic cycle of nucleoside monophosphate kinases, *Structure 3*, 483−490.
21. Billeter, S. R., Webb, S. P., Agarwal, P. K., Iordanov, T., and Hammes-Schiffer, S. (2001) Hydride transfer in liver alcohol dehydrogenase: Quantum dynamics, kinetic isotope effects, and role of enzyme motion, *J. Am. Chem. Soc. 123*, 11262−11272.
22. Eisenmesser, E. Z., Bosco, D. A., Akke, M., and Kern, D. (2002) Enzyme dynamics during catalysis, *Science 295*, 1520−1523.
23. Antoniou, D., Caratzoulas, S., Kalyanaraman, C., Mincer, J. S., and Schwartz, S. D. (2002) Barrier passage and protein dynamics in enzymatically catalyzed reactions, *Eur. J. Biochem. 269*, 3103−3112.
24. Knapp, M. J., and Klinman, J. P. (2002) Environmental coupled hydrogen tunneling. Linking catalysis to dynamics, *Eur. J. Biochem. 269*, 3113−3121.
25. Yousef, M. S., Fabiola, F., Gattis, J. L., Somasundaram, T., and Chapman, M. S. (2002) Refinement of the arginine kinase transition-state analogue complex at 1.2 Å resolution: mechanistic insights, *Acta Crystallogr., Sect. D: Biol. Crystallogr. 58*, 2009−2017.
26. Matoba, Y., and Sugiyama, M. (2003) Atomic resolution structure of prokaryotic phospholipase A_2: Analysis of internal motion and implication for a catalytic mechanism, *Proteins: Struct. Funct. Genet. 51*, 453−469.
27. Hur, S., and Bruice, T. C. (2003) The near attack conformation approach to the study of the chorismate to prephenate reaction, *Proc. Natl. Acad. Sci. U.S.A. 100*, 12015−12020.
28. Schmidt, A., and Lamzin, V. S. (2005) Extraction of functional motion in trypsin crystal structures, *Acta Crystallogr., Sect. D: Biol. Crystallogr. 61*, 1132−1139.
29. Sola, R. J., and Griebenow, K. (2006) Influence of modulated structural dynamics on the kinetics of α-chymotrypsin catalysis. Insights through chemical glycosylation, molecular dynamics and domain motion analysis, *FEBS J. 273*, 5303−5319.
30. Hammes-Schiffer, S., and Benkovic, S. J. (2006) Relating protein motion to catalysis, *Annu. Rev. Biochem. 75*, 519−541.
31. Rigden, D. J., Littlejohn, J. E., Joshi, H. V., de Groot, B. L., and Jedrzejas, M. J. (2006) Alternate structural conformations of *Streptococcus pneumoniae* hyaluronan lyase: insights into enzyme flexibility and underlying molecular mechanism of action, *J. Mol. Biol. 358*, 1165−1178.
32. Shapiro, Y. E., and Meirovitch, E. (2006) Activation energy of catalysis-related domain motion in *E. coli adenylate kinase*, *J. Phys. Chem. 110*, 11519−11524.
33. Olssen, M. H. M., Parson, W. W., and Warshel, A. (2006) Dynamical contributions to enzyme catalysis: Critical tests of a popular hypothesis, *Chem. Rev. 106*, 1737−1756.
34. Grueninger, D., and Schulz, G. E. (2007) Substrate spectrum of L-rhamnulose kinase related to models derived from two ternary complex structures, *FEBS Lett. 581*, 3127−3130.
35. Kabsch, W. (1993) Automatic processing of rotation diffraction data from crystals of initially unknown symmetry and cell constants, *J. Appl. Crystallogr. 26*, 795−800.
36. Brünger, A. T., Adams, P. D., Clore, G. M., DeLano, W. L., Grosse-Kunstleve, R. W., and Jiang, J. S. (1998) Crystallography & NMR system: a new software suite for macromolecular structure determination, *Acta Crystallogr., Sect. D: Biol. Crystallogr. 54*, 905−921.
37. Emsley, P., and Cowtan, K. (2004) Coot: model-building tools for molecular graphics, *Acta Crystallogr., Sect. D: Biol. Crystallogr. 60*, 2126−2132.
38. Murshudov, G. N., Vagin, A. A., and Dodson, E. J. (1997) Refinement of macromolecular structures by the maximum-likelihood method, *Acta Crystallogr., Sect. D: Biol. Crystallogr. 53*, 240−255.
39. Winn, M. D., Isupov, M. N., and Murshudov, G. N. (2001) Use of TLS parameters to model anisotropic displacements in macromolecular refinement, *Acta Crystallogr., Sect. D: Biol. Crystallogr. 57*, 122−133.
40. Howlin, B., Butler, S. A., Moss, D. S., Harris, G. W., and Driessen, H. P. C. (1993) TLSANL: TLS parameter-analysis program for segmented anisotropic refinement of macromolecular structures, *J. Appl. Crystallogr. 26*, 622−624.
41. Fenn, T. D., Ringe, D., and Petsko, G. A. (2003) POVscriptC: a program for model and data visualization using persistence of vision ray-tracing, *J. Appl. Crystallogr. 36*, 944−947.

BI7012799